J. Inst. Eng. India Ser. A (September 2016) 97(3):231–238
DOI 10.1007/s40030-016-0179-6

ORIGINAL CONTRIBUTION

Characterization and Evaluation of Micro-mechanical Properties of Ultra High Strength Concrete by using Micro-indentation Test

A. Ramachandra Murthy[1] · Nagesh R. Iyer[1] · B. K. Raghu Prasad[2]

Received: 17 November 2012 / Accepted: 1 September 2016 / Published online: 26 September 2016

Abstract This work presents the details of characterization and micro-mechanical properties of ultra high strength concrete. Characterization was carried out for High Strength Concrete (HSC, HSC1) and Ultra High Strength Concrete (UHSC). Various mechanical properties, namely, compressive strength, split tensile strength and modulus of elasticity have been estimated for HSC, HSC1 and UHSC. It was observed from characterization studies that the split tensile strength is high in the case of UHSC compared to HSC and HSC1. X-ray diffraction analysis has been performed for cement, silica fume and quartz powder to know the chemical composition. The amount of quantified phases has been estimated. Micro indentation technique has been employed to evaluate the micromechanical properties such as modulus of elasticity and hardness. Oliver and Pharr method has been used to compute modulus of elasticity and hardness. It is observed that the value of modulus of elasticity obtained from the micro indentation test is in very good agreement with that of the value obtained from uniaxial compression test data of a cylindrical specimen. Finally micro-structure of the specimen has been obtained for various magnifications to examine the voids/pores in the UHSC matrix.

Keywords High strength concrete · Ultra high strength concrete · Micro-indentation · XRD analysis · Micro-structure

✉ A. Ramachandra Murthy
murthyarc@serc.res.in

[1] CSIR-Structural Engineering Research Centre, Taramani, Chennai 600113, India

[2] Department of Civil Engineering, Indian Institute of Science, Bangalore, India

Introduction

Concrete has been one of the most commonly used construction materials in the world. One of the major problems civil engineers face today is concerned with preservation, maintenance and retrofitting of structures. The historical development of concrete material may be marked and divided into several stages. The first is the traditional Normal Strength Concrete (NSC) where only four kinds of ingredients, namely, cement, water, fine aggregates and coarse aggregates are used. With the increasing development in physical infrastructure, such as high-rise buildings, long-span bridges, flyovers, power plant structures, higher compressive strength concrete is preferred in most cases. When the compressive strength of concrete is generally higher than 50 MPa, it is usually defined as high strength concrete. The easiest way to reach high compressive strength is to reduce the water–cement ratio. Therefore, in HSC, the fifth ingredient, the water reducing agent or superplasticizer, is found to be indispensable. However, sometimes the compressive strength is not as important and necessary as some other properties, such as low penetrability, high durability and excellent workability. Thus, High Performance Concrete (HPC) was proposed and widely studied at the end of the last century. Currently, an UHSC with axial compressive strength more than 100 MPa and also with a high tensile strength (more than 10 % of the compressive strength) has been successfully developed [1–8].

Another recent development in the study of concrete properties is the use of nanotechnology. Nanotechnology has been developing rapidly in all the science and engineering fields. The introduction of nanotechnology application into the domain of construction materials has started in the recent years [9]. Micro-indentation method has

become a useful method for evaluation of micro-mechanical properties such as micro hardness and elastic modulus. The researchers have [10] employed the depth sensing microindentation technique to evaluate the elastic modulus and micro-strength of the Interfacial Transition Zone (ITZ) around steel reinforcement in practical reinforced concrete. Some of the previous investigators have [11] evaluated the mechanical properties, particularly the elastic modulus and the hardness of the major phases of Portland cements (C_3S and alite, C_2S and belite, C_3A, C_4AF) measured at the microscopic scale by nanoindentation and at the macroscopic scale by the resonance frequencies technique. It has been [12] evaluated earlier mechanical durability properties of a polymer concrete using a Vickers indentation technique. Some of the researchers have [13] estimated the characteristics of the profiles of elastic modulus and hardness of the steel fiber–matrix and fiber–matrix–aggregate interfacial zones in steel fiber reinforced mortars were investigated by using nanoindentation and Scanning Electron Microscopy (SEM),

In the present study, three different mixes namely, high strength concrete and UHSC are characterized and their mix proportions have been arrived at using appropriate method and several trials. The properties of materials, mix proportions, mechanical properties, XRD analysis and micro mechanical properties of concrete mix have been evaluated.

Properties of Materials

The materials used for the development of HSC, HSC1 and UHSC and their corresponding mechanical properties are, for HSC, the ingredient materials are Portland cement, coarse aggregate, fine aggregate and water, whereas for HSC1, the materials are Portland cement, silica fume, quartz sand, high range water reducer, water and steel fibers. Further, for UHSC, the materials are Portland cement, silica fume, quartz sand, quartz powder, high range water reducer, water and steel fibers. The main difference between HSC1 and UHSC is the absence of quartz powder in the case of HSC1 mix. The properties of the ingredient materials used to develop HSC, HSC1 and UHSC are given in Table 1.

Table 1 Properties of materials

Cement (ordinary Portland cement)	
Grade	53 (OPC)
Specific gravity	3.15
Particle size range	31–7.5 μm
Normal consistency	28 %
Initial Setting Time	110 min
Final setting time	260 min
Compressive strength	
3—Days strength	29 MPa
7—Days strength	34 MPa
28—Days strength	57 MPa
Silica fume (SF)	
Specific gravity	2.2
Particle size range	0.2–25 μm
Percentage of passing	92 % (45 μm sieve in wet sieve analysis)
Quartz powder (QP)	
Specific gravity	2.61
Particle size range	2.3–75 μm
Percentage of passing	52 % (45 μm sieve in wet sieve analysis)
Quartz sand	
Specific gravity	1.2
Particle size range	400–800 μm
Steel fibers	
Specific gravity	7.8
Length	13 mm
Diameter	0.18 mm
Yield stress	1500 MPa
Standard sand	
Specific gravity	2.65
Particle size range	0.5–0.09 mm (Grade 3 of IS:650)
Coarse aggregate	
Specific gravity	2.8
Particle size range	4.75–20 mm
Super plasticizers (SP)—polycarboxylate ether based superplasticizer is used	
Appearance	Light yellow coloured liquid
pH	6.5
Volumetric mass at 20 °C	1.06 kg/l

Mix Proportion

Mix design has been carried out for HSC (M40 grade) as per Bureau of Indian Standards (BIS). In the absence of a well established comprehensive method for the design of HSC1 and UHSC, mixes have been arrived at based on several trials to get the desired strength. Information on UHSC regarding mix design to obtain the required target strength is scarce in literature. Therefore, several trials had to be tried before a final mix design. The final mix proportions and ratio obtained are given in Table 2.

Specimen Preparation

- A Hobart mixer machine (15 kg capacity) or Eirich type mixer (150 l capacity) is used to mix the concrete mixtures.

Table 2 Mix ratio of HSC, HSC1 and UHSC

Mix	Cement	Fine aggregate	Coarse aggregate	Silica fume	Quartz sand	Quartz powder	Steel fiber	w/c	SP, %
HSC	1	1.25	2.48	–	–	–	–	0.45	–
HSC1	1	–	–	0.25	1.5	–	2 %	0.33	2.5
UHSC	1	–	–	0.25	1.1	0.4	2 %	0.23	3.5

- Well mixed dry binder powder is then slowly poured into the bowl while the mixer is rotating at a slow speed.
- The speed of the mixer is increased and the mixing process is continued for about 2–3 min.
- Water is then added.
- Additional mixing is performed at this speed until a uniform mixture is achieved.
- In the case of HSC1 and UHSC, fibers are added after mixing all the ingredients such as cement, quartz sand, quartz powder and silica fume with water and superplasticizer.
- Fresh mixture is poured into the moulds using a steel scoop.
- Compaction is done by placing the filled moulds on a laboratory table vibrator for about 2 min.
- The specimens are demoulded after a lapse of 24 h.
- In case of HSC, as usual curing is done till testing, but for HSC1 and UHSC specimens, immediately after demoulding, the specimens are fully immersed in potable water at room temperature for 2 days. After 2 days of normal water curing, the specimens are placed in a autoclave and maintained at 90 °C for 2 days. The specimens are placed in oven and maintained at 200 °C for 1 day followed by autoclave curing for 2 days.

Mechanical Properties

Various mechanical properties such as compressive strength, spilt tensile strength of HSC, HSC1 and UHSC mix at 28 days are shown in Table 3. From Table 3, it can be observed that the split tensile strength for the case of HSC is 4.0 MPa. It is about 7 % of compressive strength. In the case of HSC1, the split tensile strength is about 18 % of compressive strength. The increase in strength is large compared to HSC. The increase in strength may be due to various sizes of ingredients and steel fibres. Further, it can be observed from Table 3 that UHSC has high compressive strength and tensile strength. The high strengths can be attributed to the contribution at different scales viz., at the meso scale due to the fibers and at the micro scale due to the close packing of grains which is on account of good grading of the particles.

XRD Analysis of Ingredients of UHSC

The phase identification and crystalline nature of the samples have been analyzed through XRD and the details are given in the literature [14, 15]. The materials such as cement, quartz powder and silica fume have been studied for XRD analysis. Cement, quartz sand, and silica fume samples are finely ground using mortar and pestle, and then passed through 25 micron sieve, in order to avoid preferred orientation. Sample preparation is a main key step for quantitative analysis for influencing the sharp signal of related X-ray diffraction of indented sample. Preparation of sample is shown in Fig. 1.

After sample preparation, the samples have been subjected to XRD analysis in the range of 10–70 (2θ). Brucker's D2-Phaser, a desk top XRD have been used for analysis of sample. Copper K_α radiation is used and the power of X-ray generation is 30 kV, 10 mV. Figure 2 shows the loading of sample on the sample stage.

After collecting the XRD data, the recorded spectrum has been matched with International Centre for Diffraction Data (ICDD) based on their PDF card number, because this is a unique finger print for particular material. Further, Rietveld refinements has been done using pattern analysis software namely Total Pattern Analysis Software (TOPAS). The diffraction patterns of cement, quartz powder and silica fume have been collected. Figure 3 shows the diffraction pattern of cement, each peak corresponds to their individual phases. From Fig. 4, the

Table 3 Mechanical properties of HSC, HSC1 and UHSC

S. no.	Mix	Compressive strength, MPa	Split tensile strength, MPa	Modulus of elasticity, MPa
1.	HSC	57.14	3.96	35,780
2.	HSC1	87.71	15.38	37,890
3.	UHSC	122.52	20.65	42,987

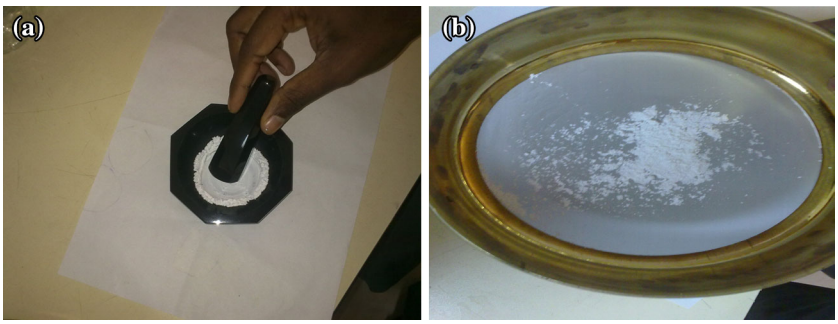

Fig. 1 Preparation of sample for XRD. **a** Grinding samples using mortar and pestle. **b** Sieving the sample through 25 μ sieve

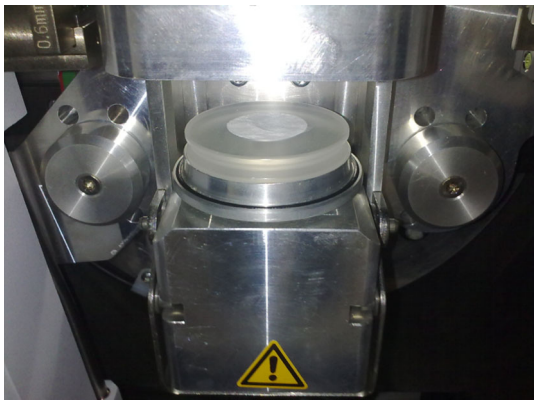

Fig. 2 Sample loading

diffraction pattern of quartz, it can be clearly understood that the sample has crystalline nature of the quartz in the bulk powder. The amorphous nature of silica fume (due to amorphous peak in XRD) can be inferred from Fig. 5 and small humps of peaks indicate the presence of small amount of quartz in the bulk.

From the Figs. 3, 4 and 5, the quantitative amount of individual phase has been estimated. The quantified phase in the cement are C_3S—47.90 %, C_2S—21.50 %, C_3A—3.13 %, C_4AF-14.37 %, Calcite-8.04 %, Gypsum-1.69 %, Lime 0.12 %, Magnesite-3.01 %, Periclase-0.43 %, Quartz-1.19 %, Rutile-0.15 %. For Quartz powder, the amounts of constituent phases are Quartz-99.85 %, Cristobalite-0.15 % and for silica fume, the values are quartz-34.29 % and cristoballite-65.71 %.

Micro Mechanical Properties of UHSC using Micro-indentation Technique

Micro indentation testing is based on forcing an indenter into the surface of the material and determining the response in terms of size of indentation. A typical load-indenter penetration depth curve obtained during loading–unloading cycle in the micro indentation test is shown in Fig. 6 which is analysed using

$$S = \frac{dp}{dh} = \frac{2}{\sqrt{\pi}}\sqrt{A} \tag{1}$$

Here, S = dP/dh is the experimentally measured stiffness of the upper portion of the unloading data and A is the projected area of the elastic contact. E_r is the reduced modulus which accounts for elastic displacements in both the sample and the indenter and is defined by,

Fig. 3 XRD pattern of cement

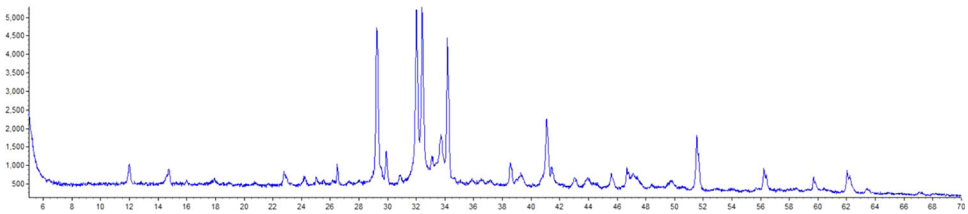

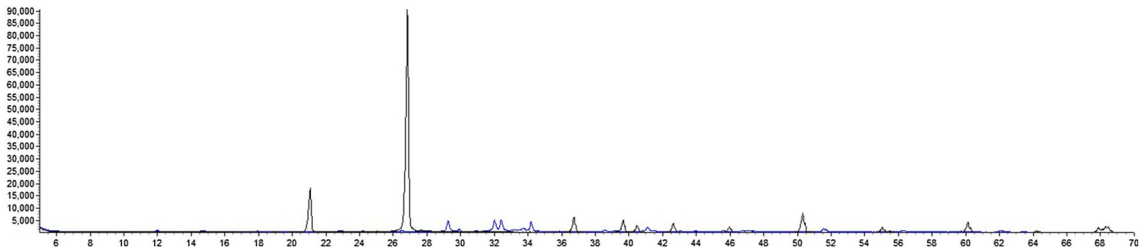

Fig. 4 XRD pattern of quartz powder

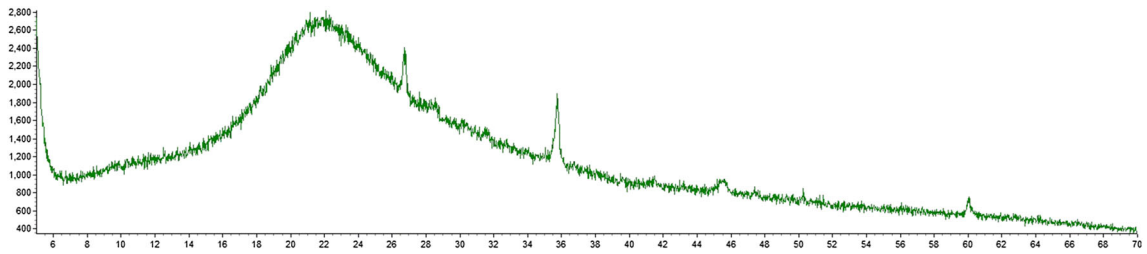

Fig. 5 XRD pattern of silica fume

$$\frac{1}{E_r} = \frac{1-v^2}{E} + \frac{1-vi^2}{E_i} \tag{2}$$

where, E and ν are Young's modulus and Poisson's ratio respectively for the specimen and E_i and ν_i are the same parameters for the indenter, respectively [16, 17]. The main parameters for determination of Young's modulus and the hardness are the maximum load (P_{max}), the maximum depth (h_{max}), and the initial unloading contact stiffness ($S = dP/dh$), to be measured only at peak load. From Eq. 3,

$$E_r = \frac{\sqrt{\pi}}{2}\frac{S}{\sqrt{A}} \tag{3}$$

which relates the reduced modulus, E_r, to the contact area, A. The area of contact at peak load is determined by the geometry of the indenter and the depth of contact, h_c. The parameters and terminologies related to the depth of indentation and used hereafter for analysis are explained in Fig. 7, which shows the cross-section of an indentation with the position and movement of indenter at different stages of loading. Stage-1 is the initial position before indentation ($P = 0$), stage-2 is the point where loading is maximum (P_{max}) and the depth of penetration is also maximum (h_{max}). Stage-3 is the unloading portion in which the indenter moves upwards and the elastic recovery of depth takes place. In stage-4, the indenter is removed completely from the specimen and the indentation depth reduces from h max to a final depth h_f. At any time during loading, the maximum displacement h_{max} can be written as,

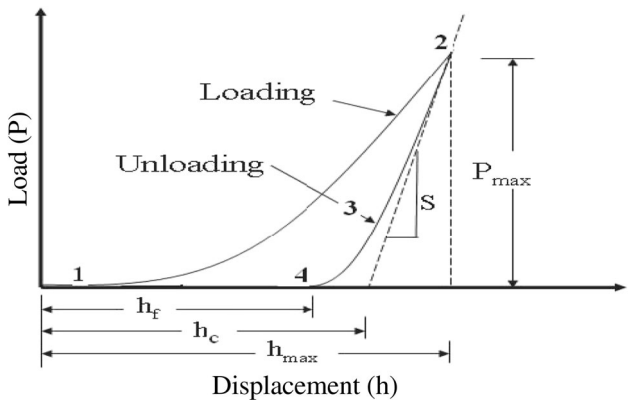

Fig. 6 Typical load against indentor penetration curve from micro-indentation test

$$h_{max} = h_c + h_s \tag{4}$$

where, h_c is the contact depth and h_s is the surface displacement at the perimeter of the contact. By measuring the initial unloading stiffness and assuming that the contact area is equal to the optically measured area of the hardness impression (Oliver and Pharr [17]), the indenter geometry can be described by an area function F(h) which relates the cross-sectional area of the indenter to the distance from its tip, h. Given that the indenter does not itself deform significantly, the projected contact area at peak load can then be computed using,

$$A = F(h_c) \tag{5}$$

The functional form of F must be established experimentally prior to the analysis. The contact depth, h_c can be determined from the experimental data by using,

$$h_c = h_{max} - h_s \tag{6}$$

which follows directly from Eq. 5. Since h_{max} can be experimentally measured, the key to the analysis then becomes, how the displacement of the surface at the contact perimeter, h_s, can be ascertained from the load–displacement data. The deflection of the surface at the contact perimeter depends on the indenter geometry. In addition to the modulus of elasticity, the hardness (H) of the material can also be determined. The hardness is defined as the mean pressure the material will support under load, hence it can be computed using,

$$H = \frac{P_{max}}{A} \tag{7}$$

where, A is the projected area of contact at peak load evaluated from Eq. 7. The Vickers Hardness (HV) in units of MPa can be computed using [18],

$$HV = \frac{2P\mathrm{Sin}(\varphi/2)}{D^2} = 1.8544\frac{P}{D^2} \tag{8}$$

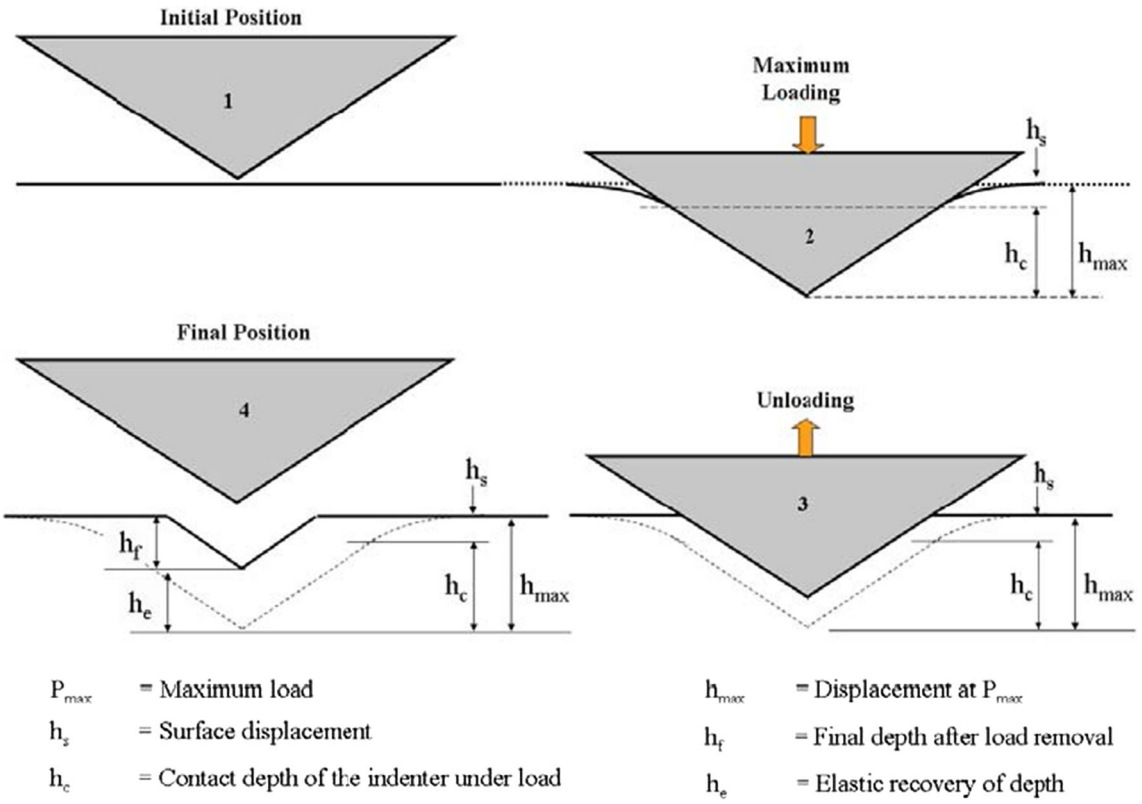

Fig. 7 Schematic of indenter penetration at different load stages

Fig. 8 Samples for micro-indentation

where, P = load (N), D = mean diagonal of indentation (mm) and $\varphi = 136°$. Since, in the case of the Vickers indenter the angle $\varphi = 136°$, the diagonal D is given by,

$$D \cong 7.0006h \tag{9}$$

Experimental Studies

Specimens having diameter of 50 mm and thickness of 10 mm have been prepared from UHSC mix. After heat treatment of the samples, dry polishing has been carried out by using 100, 180, 240, 320, 400, 600, 800 and 1000 grit silicon carbide papers. Further, polishing has been done with rotating cloth and diamond lapping film. Figure 8 shows the samples prepared for micro indentation and micro structure.

Fig. 9 Vickers pyramid diamond microscope

Figures 9 and 10 show the schematic set-up of Vickers pyramid diamond microscope and metallurgical microscope.

Average penetration depths have been recorded for various loads for all the samples. Based on the above the procedure, modulus of elasticity has been evaluated for all the specimens. Table 4 shows the values micro mechanical properties of UHSC. Figure 11a–c shows the variation of penetration depth for different specimens. From Table 4, it can be observed that the modulus of elasticity is in very

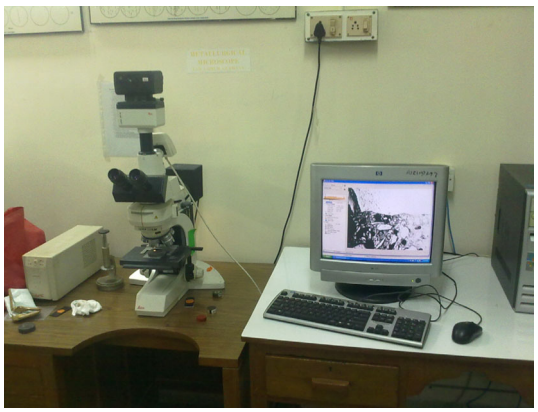

Fig. 10 Metallurgical microscope

Table 4 Micro mechanical properties of UHSC

Specimen no.	Load, gmf	Avg. penetration depth, mm	Modulus of elasticity, MPa
1	0	0	39,876.6
	10	1.739	
	15	2.186	
	25	2.668	
	50	3.185	
	100	3.528	
2	0	0	42,749.18
	10	1.652	
	15	2.231	
	25	2.765	
	50	3.232	
	100	3.789	
3	0	0	41,765.41
	10	1.701	
	15	2.301	
	25	2.823	
	50	3.301	
	100	3.652	

good agreement with that of the value obtained from uni-axial compression test data of a cylindrical specimen (refer Table 3). Figure 12 shows the micro-structure of typical UHSC specimen. From Fig. 12, it can be observed that there are some more pores/voids in the matrix of UHSC. There is scope to further improve the micro-structure of UHSC by adding cementitious/pozzolanic materials.

Conclusion

Characterization details of high strength concrete (HSC, HSC1) and ultra high strength concrete have been presented. Mix proportion for HSC has been arrived at based

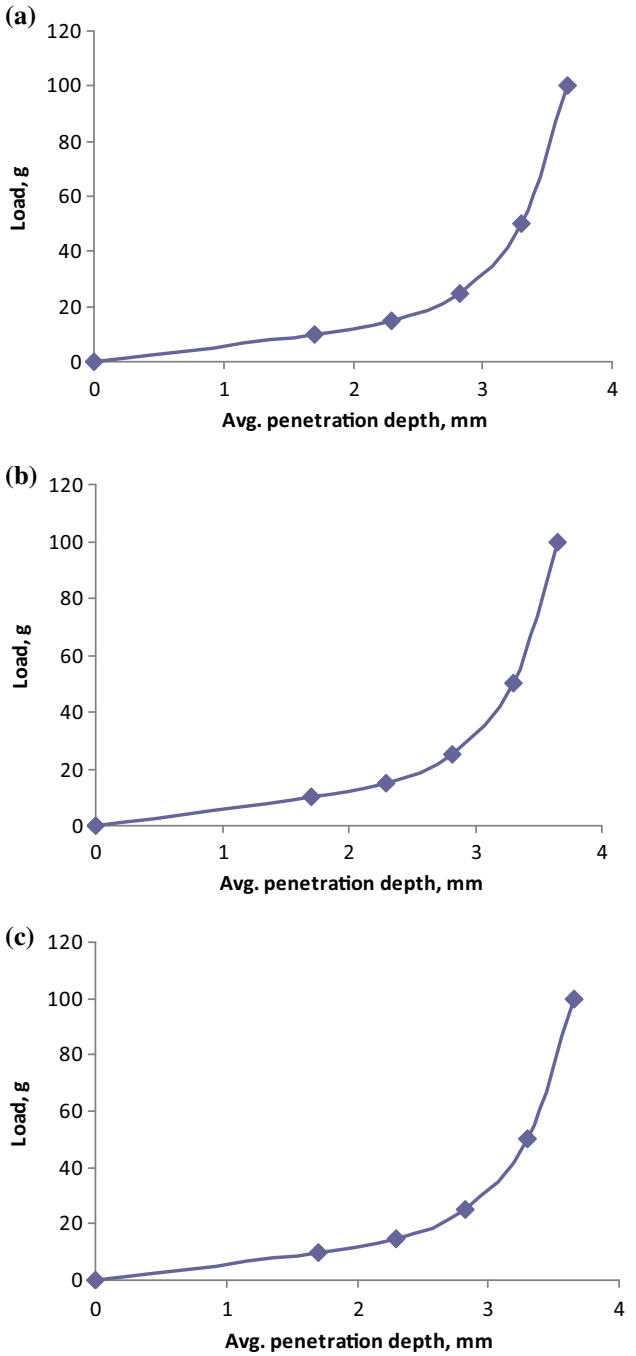

Fig. 11 Load against micro-indentation depth for **a** specimen 1, **b** specimen 2, **c** specimen 3

on BIS codes of practice whereas mix has been arrived at based on several trials for HSC1 and UHSC mix.

It was observed that the compressive strength of UHSC is about 122 MPa which is about 2 times of HSC and 1.5 times of HSC1. The split tensile strength for the case of HSC is 4.0 MPa. It is about 7 % of compressive strength. In the case of HSC1 and UHSC, the split tensile strength is about 18 % of compressive strength. The high compressive

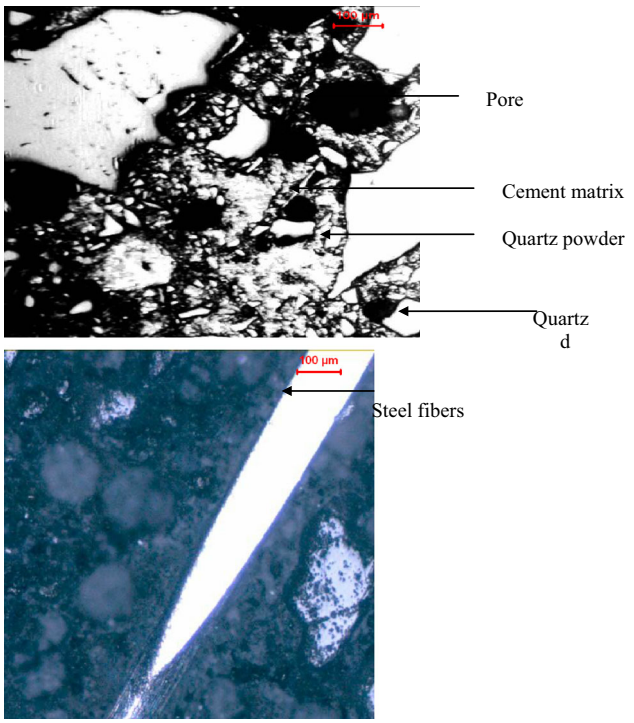

Fig. 12 Micro-structure of UHSC

strength and split tensile strength could be attributed to the contribution at different scales viz., at the meso scale due to the fibers and at the micro scale due to the close packing of grains which is on account of good grading of the particles.

XRD analysis has been performed for cement, silica fume and quartz powder to know the chemical composition. Brucker's D2-Phaser, a desk top XRD have been used for analysis of sample. From XRD analysis it was observed that the nature of silica fume is amorphous.

The modulus of elasticity obtained by using micro indentation technique was in very good agreement with that of the value obtained from uniaxial compression test data of a cylindrical specimen. From micro-structure plots, it was noted that there are some pores/voids in the UHSC matrix.

Acknowledgements The authors wish to acknowledge with thanks the valuable technical suggestions and support provided by the Computational Structural Mechanics Group, the Advanced Materials Laboratory, CSIR-Structural Engineering Research Centre, Chennai, India to carry out the experiments.

References

1. P. Richard, M.H. Cheyrezy, Composition of reactive powder concretes. Cem. Concr. Res. **25**(7), 1501–1511 (1995)
2. P. Richard, M.H. Cheyrezy, Reactive powder concretes with high ductility and 200–800 MPa compressive strength. ACI SP 144 **24**, 507–518 (1994)
3. A.N. Mingzhe, Y.U. Ziruo, M. Sun, S. Zheng, L. Liang, Fatigue properties of RPC under cyclic loads of single-stage and multi-level amplitude. J. Wuhan Univ. Technol. Mater. Sci. **25**(1), 167–173 (2010)
4. P. Goltermann, V. Johansen, L. Palbol, Packing of aggregates: an alternate tool to determine the optimal aggregate mix. ACI Mater. J. **94**(5), 435–443 (1997)
5. K. Sarkar, V. Vishal, T.N. Singh, An empirical correlation of index geomechanical parameters with the compressional wave velocity. Geotech. Geol. Eng. **30**, 469–479 (2012)
6. V. Vishal, S.P. Pradhan, T.N. Singh, Tensile strength of rock under elevated temperatures. Geotech. Geol. Eng. **29**, 1127–1133 (2011)
7. R. Singh, V. Vishal, T.N. Singh, P.G. Ranjith, A comparative study of generalized regression neural network approach and adaptive neuro-fuzzy inference systems for prediction of unconfined compressive strength of rocks. Neural. Comput. Appl. **23**, 499–506 (2012)
8. R. Singh, V. Vishal, T.N. Singh, Soft computing method for assessment of compressional wave velocity. Sci. Iran. Trans. Civil Eng. **19**(4), 1018–1024 (2012). **(Elsevier)**
9. M. Sonebi, Utilization of micro-indentation technique to determine the micromechanical properties of ITZ in cementitious materials, in *Proceedings of ACI Session on Nanotechnology of Concrete: Recent Developments and Future Perspectives*. Denver, 2006
10. W. Zhu, P.J. Bartos, Application of depth-sensing micro indentation testing to study of interfacial transition zone in reinforced concrete. Cem. Concr. Res. **30**, 1299–1304 (2000)
11. K. Velez, S. Maximilien, D. Damidot, G. Fantozzi, F. Sorrentino, Determination by nano-indentation of elastic modulus and hardness of pure constituents of Portland cement clinker. Cem. Concr. Res. **31**(4), 555–561 (2001)
12. Gian Domenico Soraru, Pierpaolo tassone, mechanical durability of a polymer concrete: a vickers indentation study of the strength degradation process. Constr. Build. Mater. **18**, 561–566 (2004)
13. X.H. Wang, S. Jacobsen, J.Y. He, Z.L. Zhang, S.F. Lee, H.L. Lein, Application of nanoindentation testing to study of the interfacial transition zone in steel fiber reinforced mortar. Cem. Concr. Res. **39**, 701–715 (2009)
14. A. Bezjak, I. Jelenic, Quantitative determination of major and minor phases in portland cements from X-ray diffraction patterns represented by fourier series. Cem. Concr. Res. **1**(5), 475–492 (1971)
15. L.P. Aldridge, Accuracy and precision of phase analysis in portland cement by bogue, microscopic and X-ray diffraction method. Cem. Concr. Res. **12**(2), 381–398 (1982)
16. S. Bueno, C. Baudin, Instrumented vickers micro indentation of alumina-based materials. J. Mater. Res. **21**(1), 161–173 (2006)
17. W.C. Oliver, G.M. Pharr, An improved technique for determining hardness and elastic modulus using load and displacement sensing indentation experiments. J. Mater. Res. **7**(6), 1564–1583 (1992)
18. M.C.A. Glinicki, M. Zielinski, Depth-sensing indentation method for evaluation of efficiency of secondary cementitious materials. Cem. Concr. Res. **34**, 721–724 (2004)